

Comparison of particle size methodology and assessment of Nanoparticle Tracking Analysis (NTA) as a tool for live monitoring of crystallisation pathways

Kate P. M. McComiskey and Lidia Tajber*

Synthesis and Solid State Pharmaceutical Centre, School of Pharmacy and Pharmaceutical Sciences, Trinity College Dublin, Dublin 2, Ireland.

*School of Pharmacy and Pharmaceutical Sciences, Trinity College Dublin, College Green, Dublin 2, Ireland. Tel: +35318962787. Fax: +35318962810. Email: ltajber@tcd.ie

Abstract

Sample complexity and polydispersity presents challenges surrounding particle size measurements for nanoparticles (NPs). To ensure the delivery of high quality products to the marketplace it is imperative that this task is performed with the greatest accuracy and certainty. For this reason, particle sizing via more than one technique is critical to the success of the formulation process. Dynamic light scattering (DLS) and nanoparticle tracking analysis (NTA) are techniques that size particles based on their Brownian motion in liquid medium. However, each technique has advantages and disadvantages associated with its application. This study was designed with the intent of comparing these techniques in a critical manner. NPs were formed using three Biopharmaceutics Classification System class II compounds: itraconazole, ketoconazole and posaconazole, using an anti-solvent addition, bottom up method. The impact of polyethylene glycol, polyethylene glycol methyl ether and polyethylene glycol dimethyl ether with a molecular weight 2000 Da, as stabilizers, was assessed using these two particle sizing techniques. Mie light scattering theory was successfully used to explain the relationship between material composition and particle scattering power. A change in material refractive index, associated with an amorphous to crystalline solid state transformation, was predominantly responsible for the observed change in the light scattering power of posaconazole nano-dispersions. The innovative application of NTA for the live tracking of these physical processes was explored for the first time. This novel finding can serve to deepen our understanding of the dynamic crystallisation pathway undertaken by a nanoparticle.

Keywords: Nanoparticle tracking analysis, dynamic light scattering, itraconazole, ketoconazole, posaconazole, crystallisation, nanoparticle

List of Abbreviations

API = active pharmaceutical ingredient

a.u. = arbitrary unit

AUC = analytical ultracentrifugation

BCS = Biopharmaceutics Classification System

Da = Dalton

DLS = dynamic light scattering

DMPEG = polyethylene glycol dimethyl ether

ESD = equivalent spherical diameter

ITR = itraconazole

KETO = ketoconazole

MPEG = polyethylene glycol methyl ether

NTA = nanoparticle tracking analysis

NP = nanoparticle

OR = Ostwald ripening

PDI = polydispersity index

PEG = polyethylene glycol

POS = posaconazole

PSD = particle size distribution

PTFE = polytetrafluoroethylene

PXRD = powder X-ray diffraction

RI= refractive index

RSD = relative standard deviation

SD = standard deviation

SEM = scanning electron microscopy

SOP = standard operating procedure

1. Introduction

In order to fully utilise the potential of nanoparticles (NPs) as drug carriers, nanoparticle characterisation must be accurate and reliable to ensure delivery of high quality products to the marketplace. The accuracy of particle size distribution measurements is dependent upon the technique employed for analysis. The inconsistency between measurements performed via different techniques increases with sample complexity and polydispersity. For this reason, it is recommended that size characterisation is performed using at least two methods that employ different sizing techniques (Bell et al., 2012; Anderson et al., 2013).

There are a number of well established particle sizing techniques currently adopted within industry, each having their own advantages and limitations. Methods should be quick to perform, low in cost whilst providing a detailed analysis of the sample in question. Traditional sizing methods include scanning electron microscopy (SEM) and dynamic light scattering (DLS), as well as size exclusion chromatography and analytical ultracentrifugation (Bootz et al., 2004; Brown and Schuck, 2006). SEM provides three-dimensional images of the particle and can therefore reveal alternative information such as particle morphology. However when employed as a sizing technique, in order to obtain statistically significant particle size distributions (PSDs) it would be necessary to measure hundreds or thousands of individual particles, unless automated analysis software were available (Bootz et al., 2004). SEM requires drying and coating of particles with a conductive layer such as gold. Therefore particle characteristics can be inherent of the preparation procedure which can have an impact upon original particle properties (McKinlay et al., 2004).

DLS sizes particles dispersed in a liquid medium based on their translational diffusion coefficient and Brownian motion. Intensity fluctuations of laser light scattered by the particles is quantified via an autocorrelation function comparing the initial scattering intensity to the intensity after specified time periods. A slow decay in the autocorrelation function is caused by the presence of large particles moving slowly; whereas fast decay indicates the presence of fast moving small particles. The diffusion coefficient can be obtained from the measured decay rate, which is directly proportional to the inverse radius of the particles via the Stokes–Einstein equation (Einstein, 1908). Hydrodynamic diameter is then calculated based upon the Stoke – Einstein equation Eq. (1):

$$d_H = \frac{kT}{3D\pi\eta} \quad \text{Eq. (1)}$$

where d_H = hydrodynamic diameter, k = the Boltzmann constant, T = temperature, D = diffusion coefficient and η = viscosity of the medium (Svedberg, 1906). DLS offers advantages in terms of speed and the need for little sample preparation. However, this technique can be problematic when analysing multimodal complex dispersions with intensity based distributions being biased towards larger particles (Calzolari et al., 2011; Anderson et al., 2013). DLS has the capability of measuring the hydrodynamic diameter of particles within the range 1 nm to 10 μm .

Nanoparticle tracking analysis (NTA) has emerged in recent years as an alternative tool for NP size characterisation. Particles are sized based on their light scattering capabilities and Brownian motion when dispersed in a liquid medium. Particles in the sample scatter light projected from a laser, which is then tracked using a camera. The software tracks individual particles and determines their size using the Stokes – Einstein equation Eq. (1), therefore not only can NTA provide particle size measurements but also valuable information regarding particle concentration (Bell et al., 2012). Since individual particles are tracked, high peak to peak resolution of particle size distributions (PSDs) can be achieved (Filipe et al., 2010). NTA has the capability of accurately sizing particles between 30 nm to 1000 nm. NTA has the added bonus of instantaneous visualisation of light scattering centres (particles) which can provide key information with regards to sample homogeneity (Joubert et al., 2011). In order for particles to be tracked via NTA they must scatter light of an intensity above a certain threshold. The amount of light scattered is dictated by the particle scattering cross-section and intensity of incident light (Gallego-Urrea et al., 2011). The Mie theory and Rayleigh approximation are two approaches utilised when studying light scattering. Rayleigh scattering solely applies to small, dielectric spherical particles, whilst Mie theory entails a general scattering solution with no limit on particle size. Rayleigh scattering predominates for particles smaller than the wavelength of incident light. For particles that are larger than a wavelength, Mie scattering prevails (Hahn, 2009). Light scattering properties of materials are a result of both particle size and composition. It is therefore possible to distinguish between particles of a similar size based on their refractive indices (RI) (Gallego-Urrea et al., 2011). Filipe et al. (2010) utilised NTA for the purpose of live monitoring of heat induced protein aggregation, revealing valuable information regarding aggregation kinetics and aggregate size. Different sized populations were distinguishable based on their scattering intensities (Filipe et al., 2010). Yang et al. (2014) employed NTA for protein characterisation concluding

that scattering intensity information can be used to determine protein aggregate structure (Yang et al., 2014).

The intent of this study was to perform a critical comparison of the particle sizing techniques DLS and NTA for azole anti-fungal nano-dispersions. Techniques employed and sample characteristics will be considered in detail with regards to interpretation of data obtained. NPs were formed using three different APIs: itraconazole (ITR), ketoconazole (KETO) and posaconazole (POS). Polyethylene glycol (PEG), polyethylene glycol methyl ether (MPEG) and polyethylene glycol dimethyl ether (DMPEG) with a molecular weight 2000 Da (Dalton) were investigated as potential stabilizers at various concentrations. Previous work investigating the colloidal stability of these azole anti-fungal nano-dispersions utilised DLS alone (McComiskey et al., 2018). Results showed that DMPEG was the most effective stabilizer for all API nano-dispersions whilst ITR NPs had the greatest overall stability of all three APIs concerned. Kinetic modelling confirmed nanoparticle growth was driven by Ostwald ripening (OR). DMPEG encouraged OR for POS NPs whilst driving the crystallisation process as confirmed by solid state characterisation and morphological examination (McComiskey et al., 2018). A sharp increase in the variability associated with DLS data at specific time points was noted. It seemed possible that crystallisation of APIs was taking place during the DLS analysis, most notably for POS. Considering the anisotropic nature of crystals in contrast to amorphous materials, the application of NTA may provide a deeper insight into the crystallisation pathways by which these APIs proceed, as well as further information regarding particle concentration values. Given the additional capabilities offered by NTA technology, tracking these processes may facilitate the discovery of novel findings regarding the physical processes at play. We present the innovative application of NTA for the purpose of live monitoring of NP crystallisation pathways *in situ* for the first time during the course of this study.

2. Materials and Methods

2.1 Materials

Itraconazole (ITR) was a gift from Welding in GmbH (Hamburg, Germany). Ketoconazole (KETO) was purchased from Glentham Life Sciences Ltd. (Wiltshire, UK). Posaconazole (POS) was purchased from Glentham Life Sciences Ltd. (Wiltshire, UK). Poly(ethylene glycol) (PEG), poly(ethylene glycol) methyl ether (MPEG) and its dimethoxylated derivative (DMPEG) with average molecular weights of 2000 Da (Dalton) were purchased from Aldrich Chemical Co.,

Ltd. (Dorset, UK). Acetone Chromasolv[®] HPLC grade was obtained from Sigma Aldrich (Dorset, UK).

2.2 Methods

2.2.1 Anti-Solvent Precipitation of ITR, POS and KETO nanoparticles (NPs)

NPs were formed by rapid mixing of a solvent phase into an anti-solvent phase at 25 °C as described by McComiskey et al. (2018). Briefly, ITR NPs were formed using a solvent phase (2.01 mg/ml ITR in acetone) into an anti-solvent phase, using a 1:10 solvent to anti-solvent (v/v) ratio. POS NPs were formed by rapid mixing of a solvent phase (14.8 mg/ml POS in acetone) into an anti-solvent phase, using a 1:12.5 solvent to anti-solvent (v/v) ratio. KETO NPs were formed by rapid mixing of a solvent phase (3.75 mg/ml KETO in acetone) into an anti-solvent phase, using a 1:10 solvent to anti-solvent (v/v) ratio. Polymeric stabilizers (PEG, MPEG and DMPEG) were included at the following concentrations: 0.5, (0.05 % w/v), 1 (0.1 % w/v) and 1.5 mg/ml (0.15 % w/v).

2.2.2 Nanoparticle Tracking Analysis

Size characterisation determination was performed by NTA using a NanoSight NS300 device (Malvern Instruments), equipped with a red laser 638 nm and sCMOS camera. Data collection and analysis was performed using NTA 3.0 software. Anti-solvent (deionised water/stabilizer solution) and solvent (API/acetone) phases were kept at 25 °C, solutions were filtered using 0.45 µm polytetrafluoroethylene (PTFE) filters (VWR, Ireland) prior to NP formation and injected using sterile syringes into the sample chamber. Samples were diluted with the appropriate anti-solvent phase using a 1:17 dilution (v/v) prior to analysis in order to achieve the desired particle concentration, between 10⁷ and 10⁹ total particles/ml. Temperature was controlled at 25 °C for the duration of the study. Particle size was recorded every minute for 30 minutes, therefore a standard operating procedure (SOP) was created using standard measurement: 30 captures of 55 second duration, to account for ~ 5 second delay between each capture. The sample was advanced every minute changing the particles in view to ensure a truly representative sample of particles were measured. All measurements were performed in triplicate. Samples were measured with manual shutter and gains adjustment. Particle size was corrected for viscosity of the continuous phase. The sample chamber was manually cleaned using MilliQ water and 10% ethanol in water solution (v/v). Upon completion, no particles were visibly present in the sample chamber through the viewing window.

2.2.3 Dynamic Light Scattering (DLS)

The mean particle size of NPs were measured using the Zetasizer Nano ZS series (Malvern Instruments, UK). The software used for analysing and capturing measurements was Malvern Zetasizer software version 7.12. Mean particle size measurements were measured *in situ* using a 12 o.d. mm 1ml PCS8501 glass cuvette. All measurements were carried out at 25 °C. The analysis was performed in triplicate for each sample with mean particle diameter recorded every minute for 30 minutes. Particle size was corrected for viscosity of the continuous phase. Viscosity of the continuous phase was measured in triplicate at 25 °C using a Vibro Viscometer SV-10 (A&D, Japan).

3. Results and Discussion

Previous work on particle size analysis of the azole drugs (ITR, KETO and POS) carried out using DLS presented a number of key outcomes (McComiskey et al., 2018). ITR NPs had the best stability all API nano-dispersions, in both the presence and absence of stabilizers. DMPEG was the most effective stabilizer overall for all API nano-dispersions. For ITR NPs, DMPEG was the most effective when employed at 0.5 mg/ml concentration. In contrast, for KETO NPs DMPEG was most effective at the highest concentration 1.5 mg/ml. Increased variability around 15 minutes was observed in DLS data for KETO NPs stabilized with PEG and MPEG. This could suggest possible crystallisation and indeed KETO NPs were confirmed as PXRD crystalline at 30 minutes (McComiskey et al., 2018). PXRD analysis also confirmed that POS NPs initially formed an unstable amorphous phase, which was isolated within a few minutes of formation and then replaced by a more stable ordered crystalline phases of form I POS within 30 minutes. POS NPs had the poorest stability, with the presence of stabilizers appearing to promote crystallisation and destabilise nano-dispersions. POS NPs stabilised with MPEG were the least stable with increased variability in data observed at the earliest time of 15 minutes. This increased variability associated with the DLS pointed towards crystallisation but lacked certainty. With NPs existing as high energy, mobile entities in solution, tracking their dynamic crystallisation journey presents a challenging task. The use of NTA may facilitate efforts to continuously monitor this process. Therefore all API nano-dispersions were analysed using NTA in a manner similar to previous work carried out using DLS (McComiskey et al., 2018) to allow for comparisons to be drawn between the two sets of data generated via these different techniques.

3.1 Itraconazole

ITR particle size distributions (PSDs) shown in Fig. 1 highlight clear differences existing between data obtained using DLS and NTA.

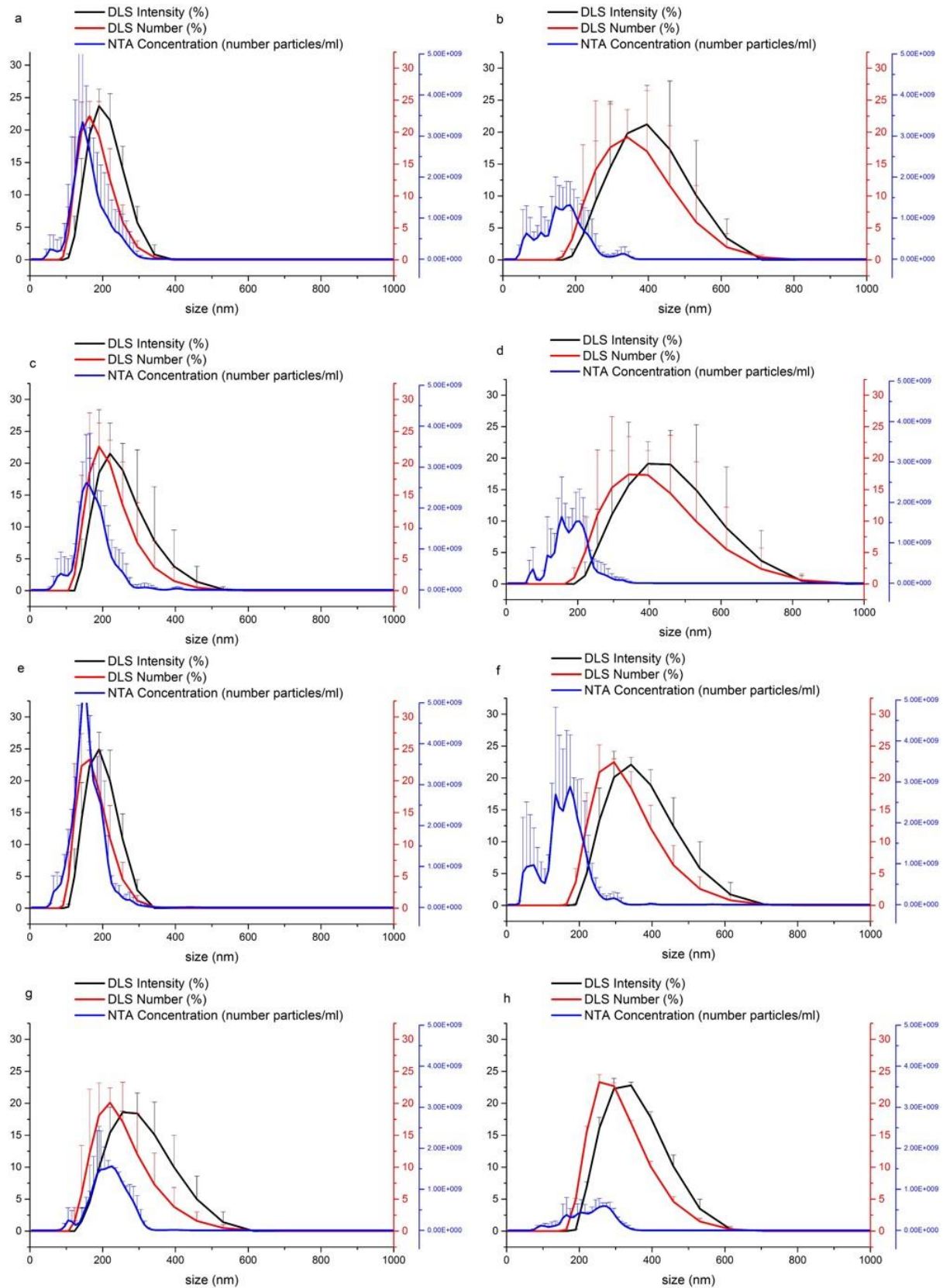


Fig. 1 ITR particle size distributions for NTA (number based) and DLS (number and intensity based) for (a) stabilizer free ITR NPs at 1 minute (b) stabilizer free ITR NPs at 30 minutes (c) ITR PEG 0.5 mg/ml NPs at 1 minute (d) ITR PEG 0.5 mg/ml NPs at 30 minutes (e) ITR MPEG 0.5 mg/ml NPs at 1 minute (f) ITR MPEG 0.5 mg/ml NPs at 30 minutes (g) ITR DMPEG 0.5 mg/ml NPs at 1 minute (h) ITR DMPEG 0.5 mg/ml NPs at 30 minutes. (n = 3)

Previous work by McComiskey et al., (2018) measured increase in particle size (%) over 30 minutes using DLS for each ITR nano-dispersion, with values ranging between 100-250%. In addition to DLS intensity based distributions, DLS number based distributions have been included for completeness (Fig. 1 and 2). However, it should be noted that these number based values have been derived from an intensity distribution. In a number based distribution, all particles within the distribution are given equal weighting irrespective of their size. In contrast, with an intensity based distribution, larger particles have the ability to skew the distribution towards larger particle sizes (Demeester et al., 2005). Therefore as expected, in all distributions number based values are lower than their intensity based equivalents obtained using DLS. For ITR PSDs at 1 minute, the three distributions are in close agreement (Fig. 1a, c, e, and g), NTA and DLS values correspond well. However at 30 minutes, the same does not remain true with a greater difference existing between the DLS and NTA distributions (Fig. 1b, d, f, and h). Interestingly, it is worth noting that the most stable ITR DMPEG 0.5 mg/ml NPs have the lowest variability for both NTA and DLS as demonstrated by the small error bars in Fig. 1g and h, indicating high measurement precision for this sample. This was also the only sample to show a decrease in variability with both techniques between minute 1 and 30 (Fig. 1g and h). Table 1 shows particle size data at 1 minute for ITR NTA versus DLS.

Table. 1 Mean particle size and size distribution measurements obtained for ITR nano-dispersions using DLS and NTA at 1 minute. (n = 3)

	DLS (intensity based)		NTA (number based)	
	Z-ave ± SD (nm)	PDI ± SD	Mean ± SD (nm)	*Concentration (number particles/ml) ± RSD
Stabilizer free ITR NPs	184 ± 10	0.04 ± 0.03	161 ± 30	2.9·10 ¹⁰ ± 20.3

ITR PEG 0.5 mg/ml	232 ± 19	0.07 ± 0.06	171 ± 18	2.5·10 ¹⁰ ± 16.0
ITR PEG 1 mg/ml	235 ± 54	0.10 ± 0.07	174 ± 28	2.0·10 ¹⁰ ± 31.0
ITR PEG 1.5 mg/ml	179 ± 21	0.11 ± 0.09	206 ± 6	2.1·10 ¹⁰ ± 11.4
ITR MPEG 0.5 mg/ml	152 ± 13	0.05 ± 0.04	153 ± 7	4.0·10 ¹⁰ ± 5.3
ITR MPEG 1 mg/ml	180 ± 7	0.02 ± 0.02	183 ± 20	2.3·10 ¹⁰ ± 19.1
ITR MPEG 1.5 mg/ml	244 ± 13	0.04 ± 0.03	205 ± 33	1.6·10 ¹⁰ ± 32.5
ITR DMPEG 0.5 mg/ml	242 ± 56	0.08 ± 0.06	202 ± 24	1.8·10 ¹⁰ ± 10.6
ITR DMPEG 1 mg/ml	246 ± 77	0.13 ± 0.03	207 ± 23	1.9·10 ¹⁰ ± 25.8
ITR DMPEG 1.5 mg/ml	179 ± 13	0.03 ± 0.03	181 ± 16	2.3·10 ¹⁰ ± 14.3

*PDI = polydispersity index, SD = standard deviation, RSD = relative standard deviation

Both techniques confirm DMPEG is the most effective stabilizer for ITR NPs at the lowest concentration of 0.5 mg/ml (Fig. 1g and h, Fig. SI. 1). Fig. 1 shows a marked decrease in NTA particle concentration between 1 minute and 30 minutes for all ITR nano-dispersions (Fig. 1 and Fig. SI. 2). ITR NTA distributions at 30 minutes appear to be multimodal and polydisperse in comparison to mono-modal distributions observed for all samples using both techniques at 1 minute (Fig. 1). However, the complexity of ITR PSDs at 30 minutes visible with NTA was not evident with DLS. This reiterates the ability of NTA to achieve greater peak resolution, distinguishing particle population's close in size, simply not possible with DLS (Filipe et al., 2010).

3.2 Ketoconazole

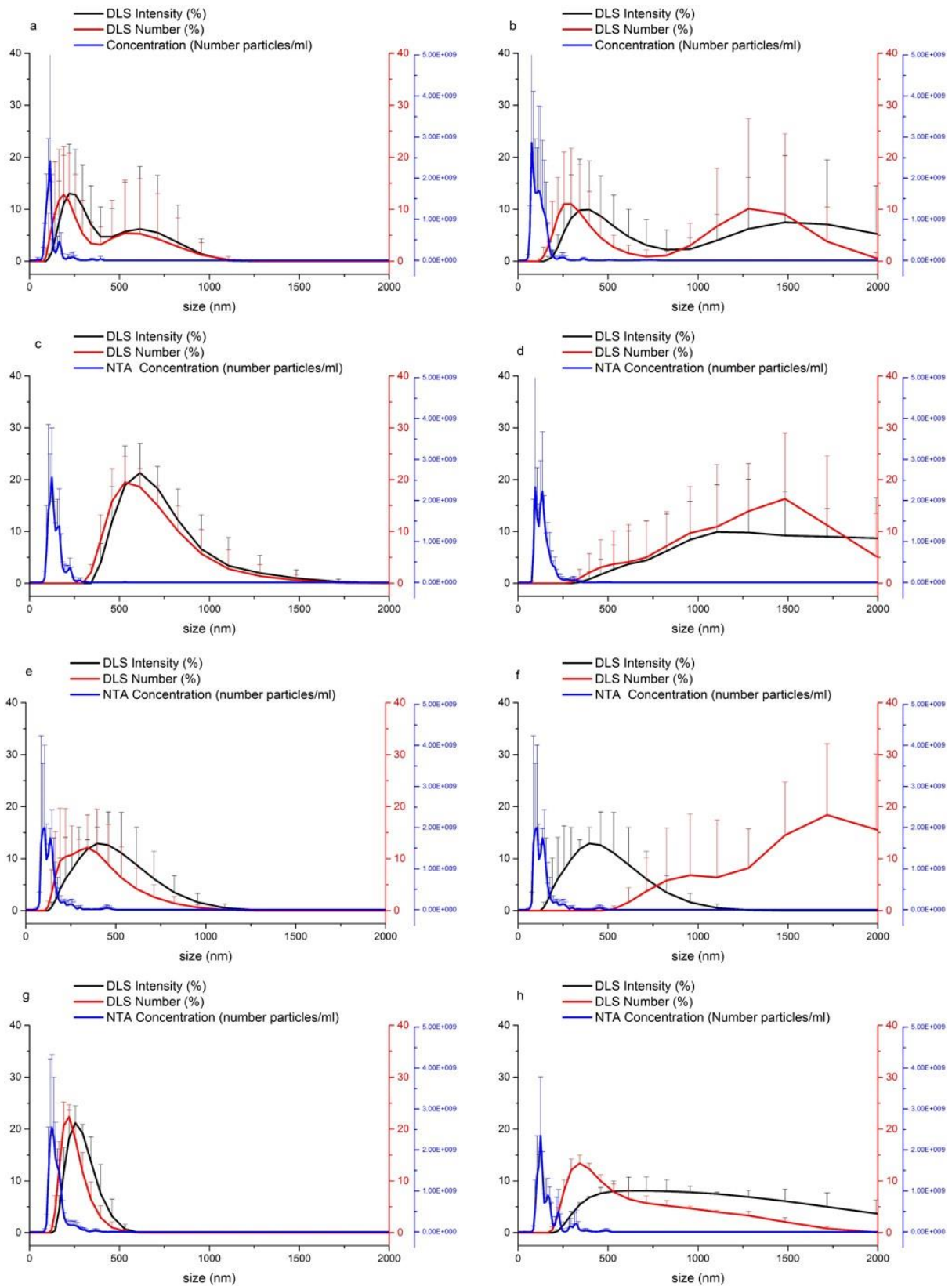


Fig. 2 KETO particle size distributions for NTA (number based) and DLS (number and intensity based) for (a) stabilizer free KETO NPs at 1 minute (b) stabilizer free KETO NPs at 30 minutes (c) KETO PEG 0.5 mg/ml NPs at 1 minute (d) KETO PEG 0.5 mg/ml NPs at 30 minutes (e) KETO

MPEG 0.5 mg/ml NPs at 1 minute (f) KETO MPEG 0.5 mg/ml NPs at 30 minutes (g) KETO DMPEG 0.5 mg/ml NPs at 1 minute (h) KETO DMPEG 0.5 mg/ml NPs at 30 minutes.

KETO particle size distributions show a great variation between DLS and NTA, with NTA sizing these samples much smaller than DLS throughout (Fig. 2). This feature has been noted elsewhere in the literature (Filipe et al., 2010). Great differences are evident at 30 minutes between the two techniques, with DLS having much broader PSDs. Large error bars are associated with both techniques for KETO distributions, indicating low measurement precision for these nano-dispersions. However, again the most stable KETO NPs containing DMPEG, have the smallest DLS error bars and variability associated with those measurements at both 1 and 30 minutes (Fig. 2g and h). There is little difference between the NTA distributions between 1 and 30 minutes for all KETO nano-dispersions, in comparison with the DLS peaks where a significant shift to a larger and broader distribution at 30 minutes was observed (Fig. 2). All other KETO nano-dispersions behaved in the same manner, with the exception being KETO DMPEG 1.5 mg/ml (Fig. Si. 3). Interestingly, this was the most the effective stabilizer for KETO nano-dispersions as confirmed by DLS. This sample was associated with the lowest variability and showed closest agreement between the two techniques (Fig. Si. 3). Table 2 contains particle size data obtained via NTA and DLS at 1 minute for KETO nano-dispersions.

Table. 2 Mean particle size and size distribution measurements obtained for KETO nano-dispersions using DLS and NTA at 1 minute. (n = 3)

	DLS (intensity based)		NTA (number based)	
	Z-ave ± SD (nm)	PDI ± SD	Mean ± SD (nm)	*Concentration (number particles/ml) ± RSD
Stabilizer free KETO NPs	204 ± 10	0.09 ± 0.07	117 ± 10	9.7·10 ⁹ ± 66.0
KETO PEG 0.5 mg/ml	639 ± 83	0.05 ± 0.04	140 ± 7	1.6·10 ¹⁰ ± 41.3
KETO PEG 1 mg/ml	658 ± 152	0.10 ± 0.07	133 ± 18	1.9·10 ¹⁰ ± 8.4
KETO PEG 1.5 mg/ml	520 ± 102	0.15 ± 0.09	153 ± 21	1.3·10 ¹⁰ ± 33.8
KETO MPEG 0.5 mg/ml	406 ± 129	0.15 ± 0.05	146 ± 10	1.5·10 ¹⁰ ± 20.7
KETO MPEG 1 mg/ml	642 ± 84	0.10 ± 0.10	133 ± 5	1.9·10 ¹⁰ ± 21.1
KETO MPEG 1.5 mg/ml	345 ± 56	0.15 ± 0.05	133 ± 7	1.1·10 ¹⁰ ± 38.2

KETO DMPEG 0.5 mg/ml	258 ± 22	0.08 ± 0.06	149 ± 13	1.7·10 ¹⁰ ± 43.5
KETO DMPEG 1 mg/ml	269 ± 24	0.14 ± 0.04	169 ± 15	1.3·10 ¹⁰ ± 46.9
KETO DMPEG 1.5 mg/ml	248 ± 14	0.10 ± 0.05	166 ± 13	2.7·10 ¹⁰ ± 15.6

*PDI = polydispersity index, SD = standard deviation, RSD = relative standard deviation

KETO particle sizes upon initial formation are much larger when measured via DLS compared with NTA equivalents (Table 2). Whilst ITR nano-dispersions show good agreement between the two techniques with particle sizes ranging between 150-250 nm (Table 1). Polydispersity index (PDI) measurements would suggest that KETO nano-dispersions are the most polydisperse of all API nano-dispersions i.e. are multimodal. This fact is also supported by the larger error bars associated with DLS data for KETO nano-dispersions compared with that of NTA (Table 2). Decreased variability associated with NTA KETO samples suggests good reproducibility for these datasets compared with DLS equivalents (Table 2). Stabilizer free KETO NPs were highlighted as being particularly unstable via DLS (McComiskey et al., 2018). This corresponds to the highest variability of all KETO nano-dispersions in particle concentration measured via NTA which can be found in Table 2. Further information regarding NTA particle concentration measurements is presented in Fig. SI. 4.

3.3 Posaconazole

Analysis of POS nano-dispersions proved to be challenging. The tendency of these samples to visibly crystallise and precipitate crystals larger than 1 micron in size within the time scale of the study, meant it was not possible to obtain size data via NTA for every time point. POS crystals visibly precipitate within 30 minutes as shown by photographs (Fig. SI. 5) and SEM images (McComiskey et al., 2018). Large crystals could be seen in the viewing field of the software causing pixel blooming and therefore obscuring smaller particles present in the sample (Fig. SI. 6a and b). In this instance, the NTA software views the large crystals as noise and will not measure their size or will attempt to size them as many small particles, an issue noted elsewhere in the literature (Gallego-Urrea et al., 2011). POS NTA particle concentration measurements shown in Table SI. 1 also displayed high variability when compared with ITR and KETO equivalents. This provides further evidence for exclusion of POS nano-dispersions from size comparisons. Therefore, particle size comparison between DLS and NTA was limited to the assessment of ITR and KETO nano-dispersions alone.

3.4 Monitoring of Crystallisation Pathways using NTA

Rayleigh approximation has been previously used by Luo et al. (2016) to explain the light scattering behaviour of gold NPs (Joubert et al., 2011; Luo et al., 2016). Due to the larger size of the ITR, KETO and POS NPs studied in this case, the same approach could not be adopted (Joubert et al., 2011; Luo et al., 2016). Therefore it seemed logical to apply Mie theory (Gallego-Urrea et al., 2011) to determine if NTA could be used to explain changes in NPs, occurring primarily due to solid state transformations and not a change in particle size. Mie scattering requires refractive index (RI) values for accurate size measurement. It is known that cubic crystals and isotropic materials can have only one RI, whilst triclinic crystals have three indices commonly denoted as α , β and γ (Carlton, 2011). The APIs in question are biaxial triclinic crystal systems, therefore having three RI values (Peeters et al., 1979, 1996, and 2004). Unfortunately, exact values for the APIs studied are not known, however a number of organic pharmaceutical materials exhibit RI values between 1.4 to above 1.7 (Watanabe and Ohnuma, 2000). For instance, sulphanilamide polymorphic forms have RI values ranging from 1.548 to 1.8 (Lin et al., 1974). Therefore, it appears that crystallisation of a particle from an isotropic phase (an amorphous form) to a triclinic crystal has the potential to be recorded by NTA technology due to changes in RI value.

This hypothesis was tested further using the Mie theory in Scatlab 1.2 software with the option "direct intensity graph" (Scatlab Project: <http://www.scatlab.org>) and scattering power as a function of size was calculated for ITR, KETO and POS based on an average RI value of 1.65 (Wong et al 2006; Palmberger et al., 2015; Touzet et al., 2018). Calculations were based on 638 nm light, the same wavelength as that used by NTA. The dispersant RI was taken as 1.33, with water being the liquid medium. The real part of the RI of the NP material was set to 1.65 and the complex part was set to 0.001, both parameters being typical of organic materials. Scattered light intensities were calculated for angles ranging 70-110°. All other parameters were left at zero (Gallego-Urrea et al., 2011). Also, scattering intensity in a range of RI values at 90° angle was calculated to reflect the triclinic nature of these APIs.

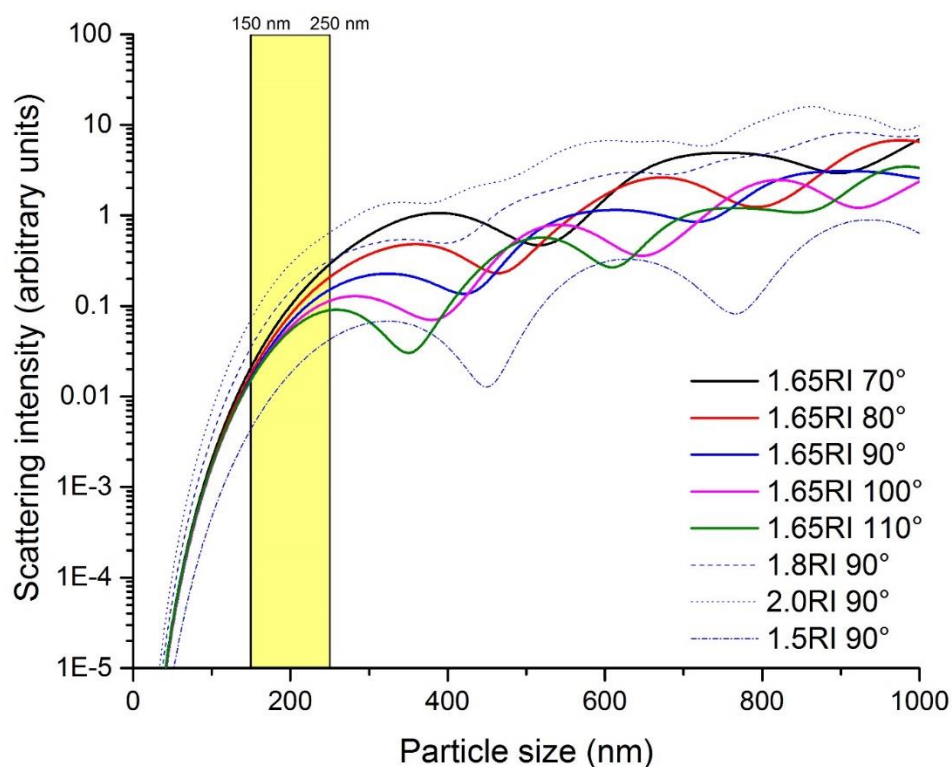


Fig. 3 Mie plot showing intensity of scattered light, calculated for the studied APIs using Mie theory in Scatlab 1.2 at a range of angles 70-110°. (yellow box highlights lowest particle size of NPs upon initial formation). RI= refractive index

This Mie plot shown in Fig. 3 demonstrates that the scattering intensity increases rapidly for smaller sized particles in contrast with larger sized particles where a plateau in intensity is reached from 200 nm and above. All APIs form NPs above 150 nm (Table 1, 2 and SI. 1). A range of RI values (1.5-2.0) were investigated, with Fig. 3 demonstrating the key impact of this parameter upon particle scattering power. Therefore we can conclude that changes in scattering intensity are predominantly dictated by material composition and not particle size. Scattergrams presented below show particle size (nm) versus the intensity (a.u.) of light scattered by NPs under analysis. It is possible to distinguish between particles of similar size based on their differing refractive indices using these graphical representations of light scattering. Particular attention should be paid to the scale of the Y-axis in the scattergrams shown.

3.4.1 Itraconazole

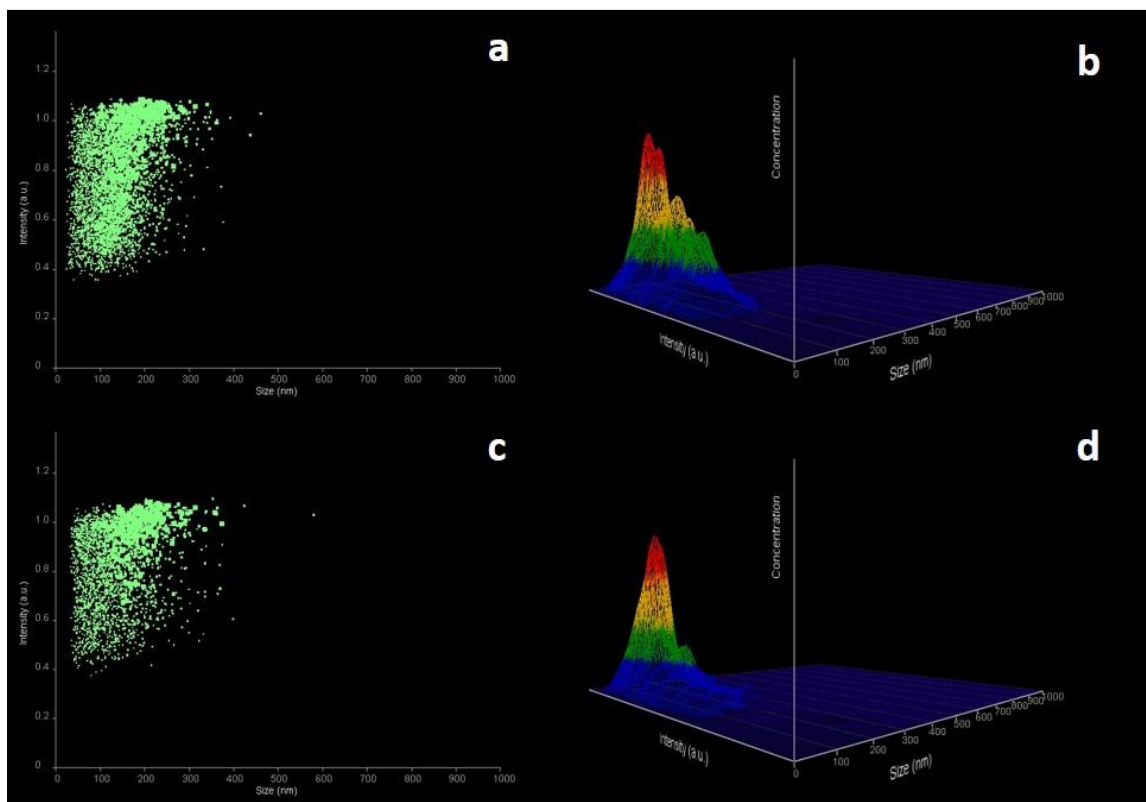


Fig. 4 NTA scattergram intensity (a.u.) vs. light with corresponding 3-D graph (size vs. intensity vs. concentration) for stabilizer free ITR NPs at (a and b) 1 minute and (c and d) 30 minutes.

ITR nano-dispersions showed little difference between 1 and 30 minutes in their scattering abilities (Fig. 4). ITR NPs scattered at the lowest level of intensity below 1.2 a.u.. ITR NPs appear X-ray disordered upon initial formation. However, these NPs are in fact liquid crystal in nature (Tarnacka et al., 2013; Mugheirbi and Tajber, 2015). An ability to flow like a liquid with some degree of long range order could reduce their ability to refract light. The greater stability of ITR nano-dispersions as confirmed by particle size measurements obtained via both techniques is supported by the stable range of light scattered throughout the 30 minutes (Fig. 4).

3.4.2 Ketoconazole

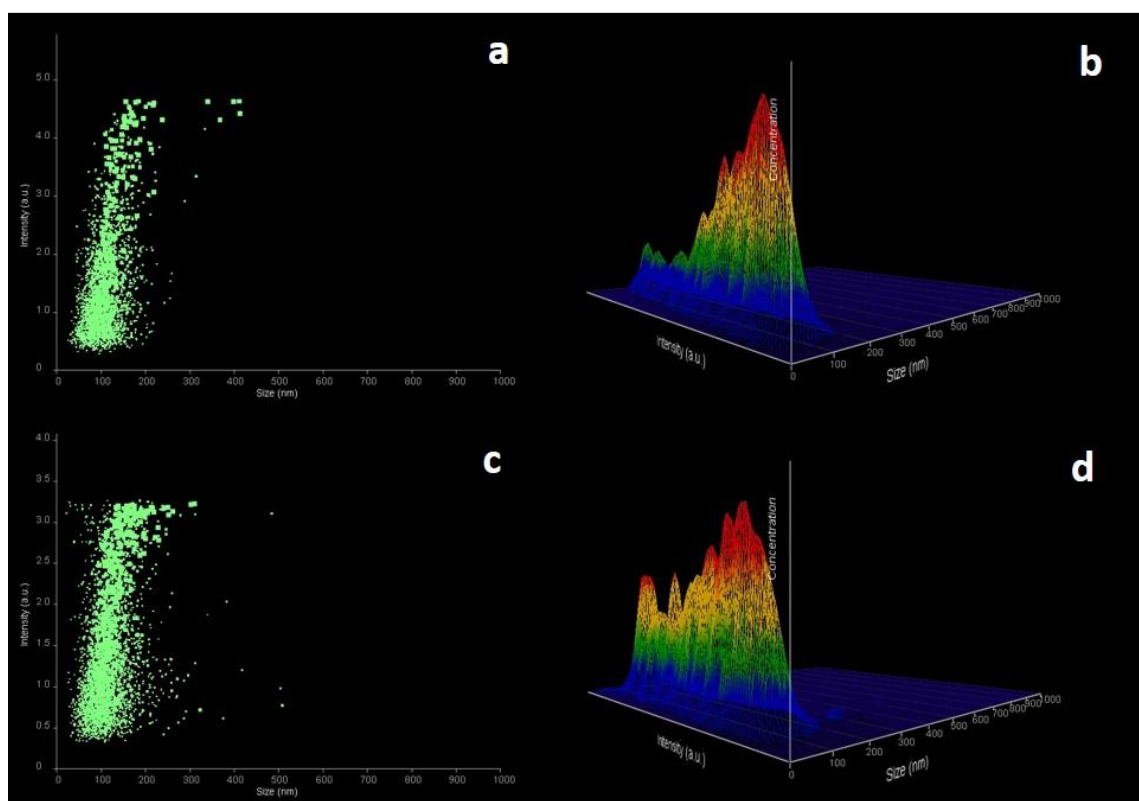


Fig. 5 NTA scattergram intensity (a.u.) vs. light with corresponding 3-D graph (size vs. intensity vs. concentration) for stabilizer free KETO NPs at (a and b) 1 minute and (c and d) 30 minutes.

Equivalent scattergrams for KETO showed a decrease in the range of intensity of light scattered by particles over the 30 minutes (Fig. 5). KETO NPs scattered light up to an intensity 5 a.u. at 1 minute, with a large sized cluster of particles scattering below 1.5 a.u. (Fig. 5a). This may suggest the presence of both amorphous and crystalline KETO NPs in this sample, with the majority being amorphous. PXRD analysis (McComiskey e al., 2018) confirms the crystalline nature of the KETO NPs at 30 minutes. An increase in the size of the particle cluster scattering at higher intensity can be seen at 30 minutes (Fig. 5c), however a significant number of particles scattering below 1.5 a.u. remain. This may suggest the simultaneous presence of both amorphous and crystalline KETO NPs at 30 minutes, with an increase in the number of crystalline particles. It is also possible that the decrease in the intensity of scattered light associated with KETO NPs can be explained by the dissolution of these particles. Wittbold and Tatarkiewicz, (2017) previously tracked the process of crystallisation and dissolution by observing varying intensity of scattered light of proteins using MANTA technology. Crystallisation was characterised by an increased intensity, whilst dissolution was represented by a decrease in the intensity of scattered light (Wittbold and Tatarkiewicz, 2017).

3.4.3 Posaconazole

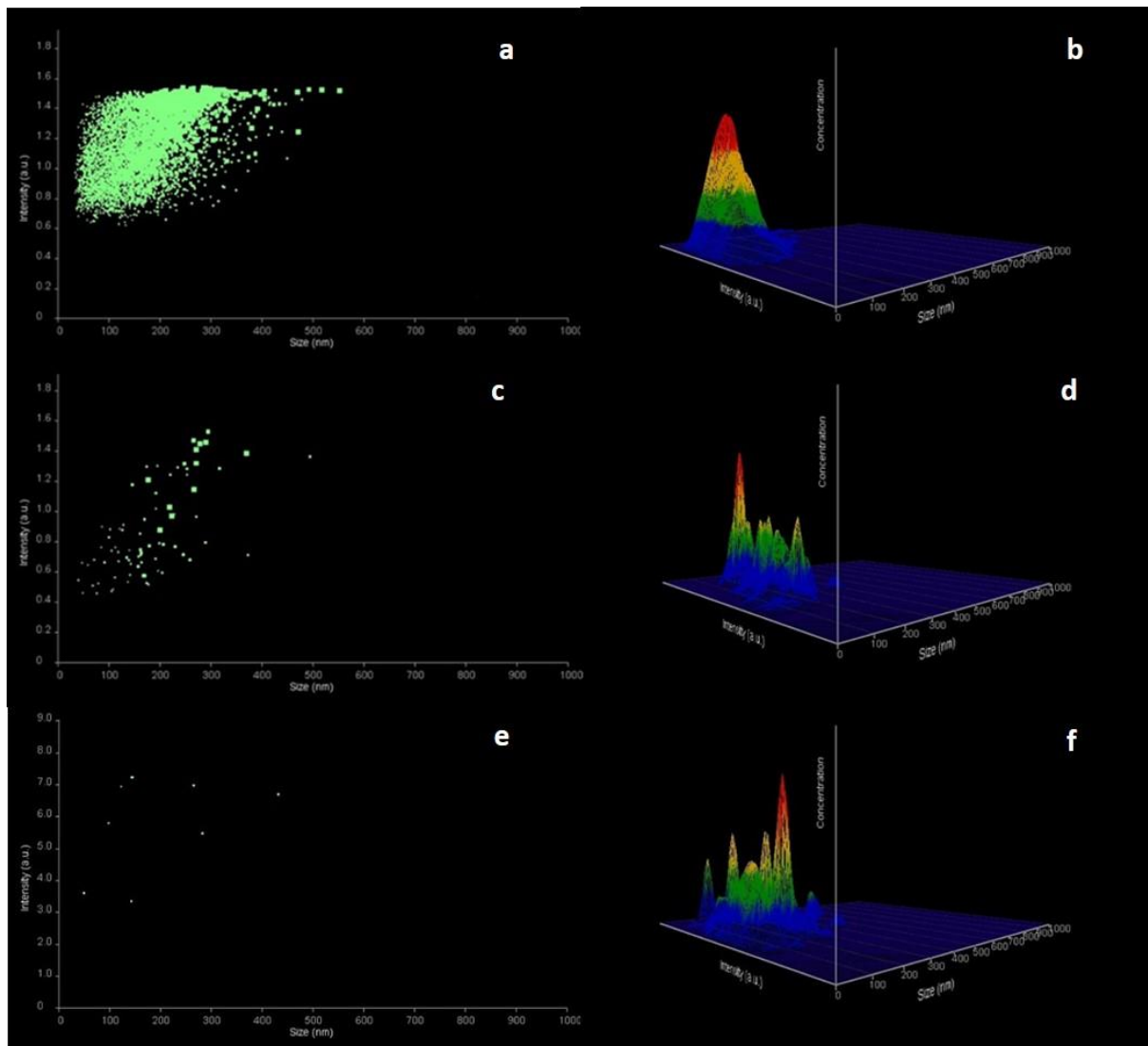


Fig. 6 NTA scattergram intensity (a.u.) vs. light with corresponding 3-D graph (size vs. intensity vs. concentration) for stabilizer free POS NPs at (a and b) 1 minute (c and d) 7 minutes and (e and f) 8 minutes.

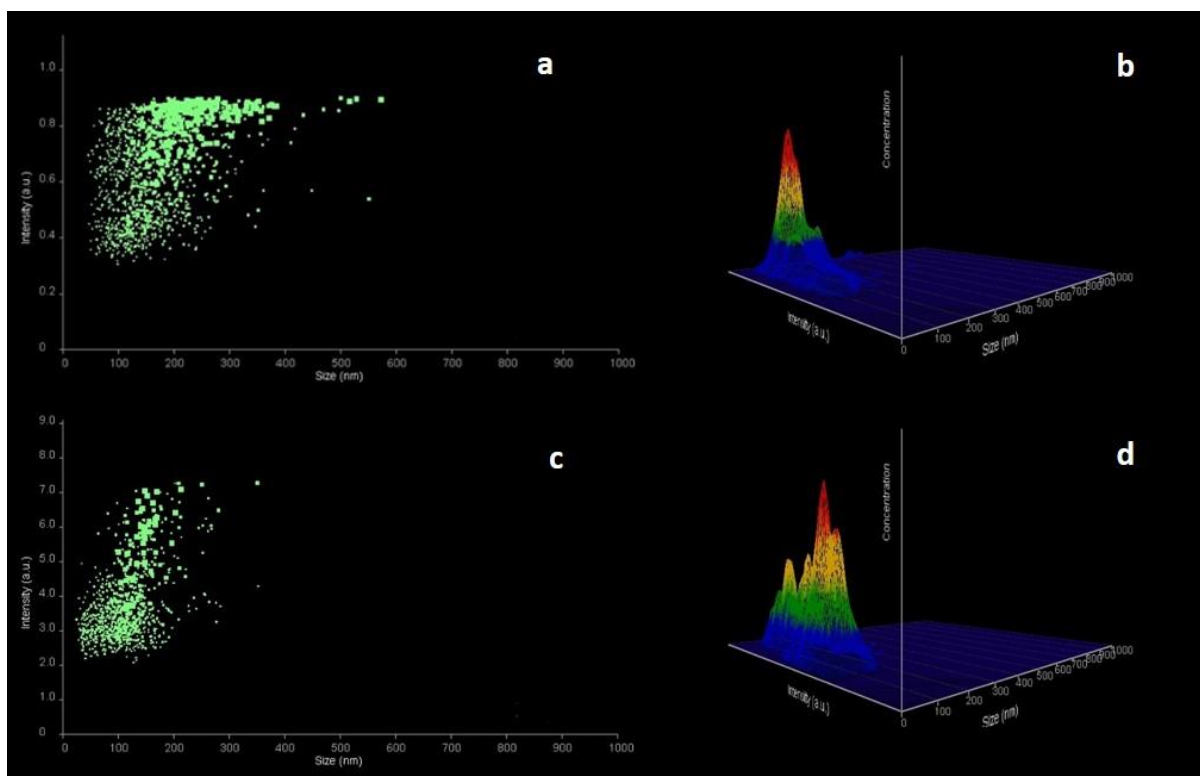


Fig. 7 NTA scattergram intensity (a.u.) vs. light with corresponding 3-D graph (size vs. intensity vs. concentration) for POS MPEG 1.5 mg/ml NPs at (a and b) 3 minutes and (c and d) 4 minutes.

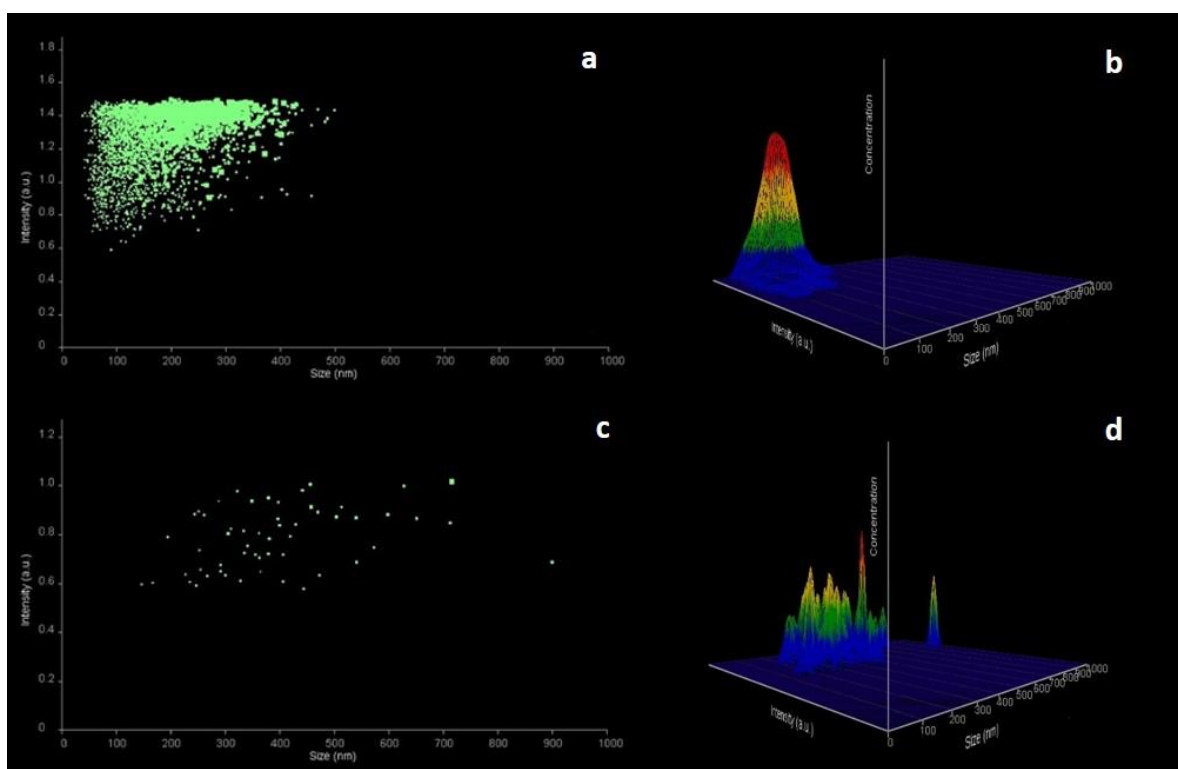


Fig. 8 NTA scattergram intensity (a.u.) vs. light with corresponding 3-D graph (size vs. intensity vs. concentration) for POS DMPEG 1 mg/ml NPs at (a and b) 1 minute and (c and d) 30 minutes.

Presented are examples of stabilizer free POS nano-dispersion (Fig. 6), as well as POS MPEG 1.5 mg/ml which crystallised the fastest (Fig. 7) and POS DMPEG 1 mg/ml which showed no signs of crystallisation over the 30 minutes (Fig. 8). Examples of scattergrams and 3-D graphs for other polymer-stabilised nano-dispersions can be found in Figs. SI. 7-24. Notably, previous work performed using DLS on these systems presented similar findings. POS MPEG 1.5 mg/ml showed signs of possible crystallisation represented by remarkable increases in particle size and variability as the experiment proceeded. In addition, POS DMPEG 1 mg/ml showed no evidence of possible crystallisation, with a consistent increase in particle size observed (McComiskey et al., 2018). A significant increase in the intensity of the light scattered by the POS NPs (refer to Y-axis) was observed over the 30 minutes of the study (Fig. 6 and 7). For all POS nano-dispersions (except POS DMPEG 1 mg/ml) prior to crystallisation particle light scattering ranges fall between 0.1 – 1.5 a.u. (Fig. 6a to 8a) compared to the scattering range 1 - 7 a.u. post crystallisation (Fig. 6e and 7c). The 3D graphs included provide a graphical representation of size versus intensity versus concentration, in this way providing information regarding the concentration of particles scattering light at particular intensities (Fig. 6 to 8). We can conclude that prior to crystallisation unstable disordered amorphous particles tend to scatter light at a decreased intensity. In contrast, post crystallisation ordered stable crystalline particles scatter light at an increased intensity. This is in agreement with the typical characteristics of amorphous materials, they are isotropic having one refractive index of light, whereas the crystalline form of POS is anisotropic having three RIs (Singh and Dunmur, 2002; Hahn et al., 2009). We can confirm that POS proceeds via a “non-classical crystallisation” pathway with evidence of initial association of these NPs in an unstructured way making them amorphous in nature, with a tendency to crystallise quickly within the 30 minute time period as shown previously by SEM and PXRD analysis (McComiskey et al., 2018). “Non-classical crystallisation” pathways involving kinetically metastable precursor particles can be found elsewhere in the literature (Niederberger and Cölfen, 2006). Amorphous-to-crystalline pathways have a thermodynamic origin. In this instance, unstable amorphous particles undergo phase transformation to a thermodynamically stable ordered crystalline phase over 30 minutes. Whereby, thermodynamically unstable phases are replaced by more stable phases (Han and Aizenberg, 2007; Pouget et al., 2009). As previously mentioned, considering Mie theory, we can conclude that the change in the light scattering power of POS NPs is caused by a change in material composition and not increased particle size. For the first time,

NTA has been successfully utilised for the innovative application of monitoring crystallisation *in situ* (Fig. 9).

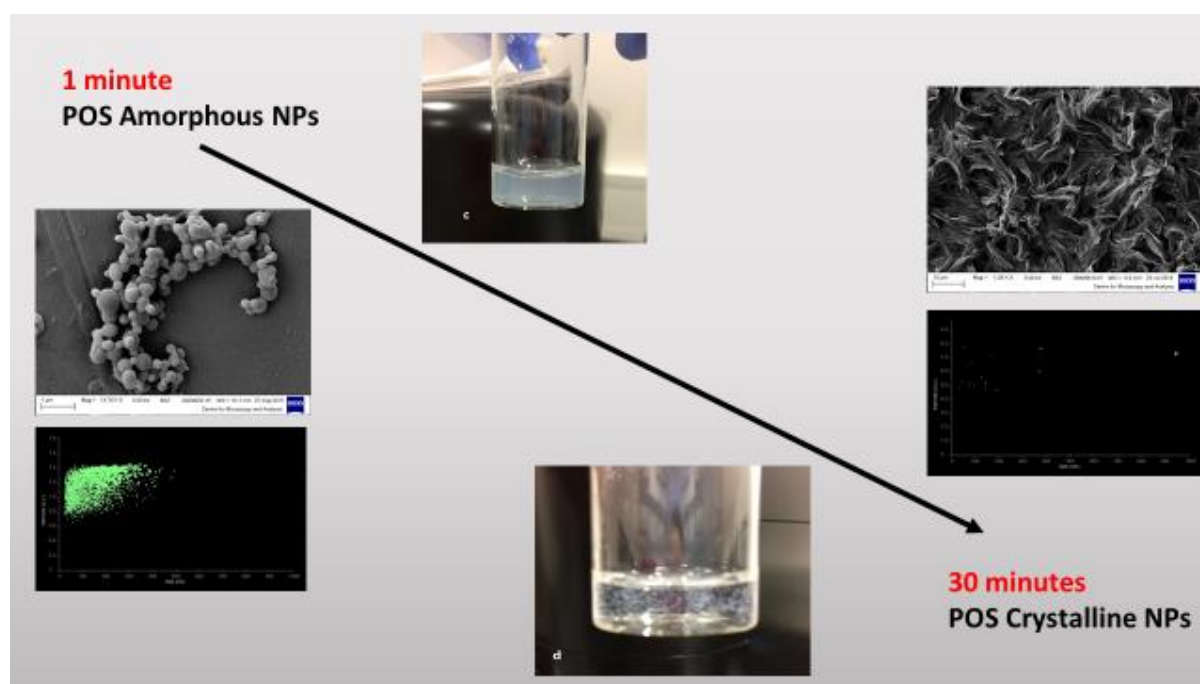


Fig. 9 Schematic representation of “non-classical crystallisation” pathway followed by POS NPs over 30 minutes of study.

Table 3 contains information regarding the time-point at which crystallisation occurs for each POS nano-dispersion. This information is also displayed in a schematic representation in Fig. 10.

Table. 3 Time-point (minutes) for crystallisation of POS nano-dispersions using NTA during 30 minutes monitoring. (n = 3)

Formulation	Time-point for crystallisation (minutes)
Stabilizer free POS NPs	7-8
POS MPEG 0.5 mg/ml	13-14
POS MPEG 1 mg/ml	9-10
POS MPEG 1.5 mg/ml	3-4
POS PEG 0.5 mg/ml	15-16
POS PEG 1 mg/ml	12-13
POS PEG 1.5 mg/ml	4-5
POS DMPEG 0.5 mg/ml	6-7
POS DMPEG 1 mg/ml	>30
POS DMPEG 1.5 mg/ml	27-28

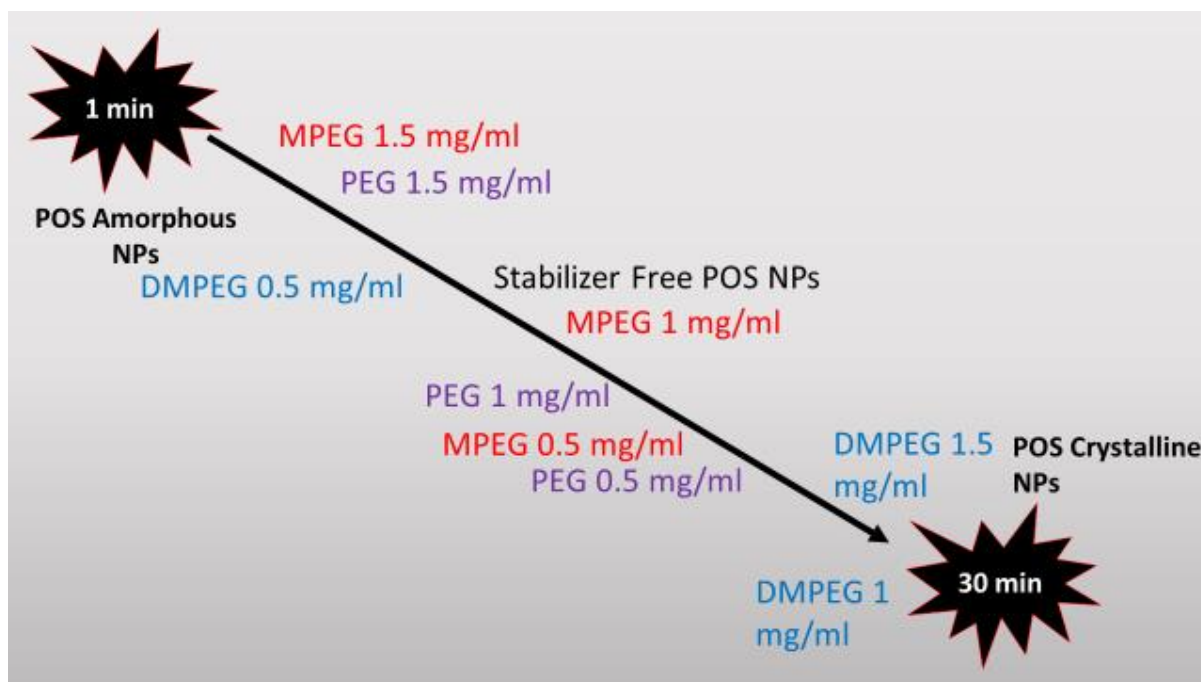


Fig.10 Schematic representation of 30 minute timeline showing point of crystallisation for POS NPs with different stabilizers.

For POS NPs stabilised by MPEG and PEG, when the stabilizer concentration is increased crystallisation occurs faster (Table 3). In other words, increasing stabilizer concentration (MPEG and PEG) appears to encourage crystallisation and the formation of ordered crystalline phases. Greater colloidal stability i.e. more efficient inhibition of crystallisation is achieved when lower concentrations of PEG and MPEG are utilised for the stabilisation of POS NPs. On the other hand, when POS NPs are stabilised by DMPEG; increasing DMPEG concentration appears to delay crystallisation. This finding is in agreement with DLS studies whereby DMPEG was the most effective stabilizer for POS nano-dispersions (Fig. SI. 25). However NTA suggests that DMPEG is most effective at a concentration of 1 mg/ml, in contrast to 1.5 mg/ml as suggested by DLS (McComiskey et al., 2018). It may be the case that increasing DMPEG concentration up to a threshold of 1 mg/ml inhibits crystallisation therefore achieving greater NP stability. Beyond this point any further increase in concentration is of no benefit, with a possible saturation limit being reached.

4. Critical Evaluation of Nanoparticle Tracking Analysis (NTA) versus Dynamic Light Scattering (DLS)

Ultimately, both NTA and DLS confirmed ITR NPs have the greatest stability. DLS confirmed DMPEG was the most effective stabilizer for ITR and KETO. This is reflected by small error bars and therefore relatively low variability associated with the NTA PSDs of these samples (Fig. 1h, 2h and Fig. SI. 3L). In general, upon initial formation ITR nano-dispersions showed the best agreement in particle size data obtained via the two techniques (Table 1). Greater differences in particle size values were observed for KETO and POS nano-dispersions at the same time point (Table 2 and SI. 1). It seems likely that the presence of larger sized particles or aggregates within samples at 30 minutes are skewing DLS distributions towards larger particle sizes (Demeester et al., 2005). This has been noted elsewhere in the literature, with the presence of few large particles within the sample obstructing the accurate size determination of the smaller dominant population (Berne and Pecora, 2000). It is also possible that some degree of particle sedimentation is occurring at 30 minutes for samples undergoing analysis, most notably for POS whereby micron sized crystals were present (McComiskey et al., 2018). For accurate size determination via both DLS and NTA, it is critical that the process of diffusion (Brownian motion) is much faster than the process of sedimentation. It is possible that larger particles present at 30 minutes may be subject to different rates of sedimentation as a consequence of their environment, which differs for DLS and NTA. This could be responsible for inconsistencies in corresponding measurements between the two techniques. It should be noted that intensity based DLS data is being compared with number based equivalents derived using NTA. Therefore, it seems that a number of large sized particles within the nano-dispersions are having profound impact on the mean particle size measured using DLS.

Fig. 1 highlighted the increase in sample complexity shown by NTA between 1 minute and 30 minutes. This confirms the ability of NTA to achieve greater peak resolution for multimodal size distributions (Dragovic et al., 2011). NTA can resolve particle populations with a 1.5 fold difference in size compared with DLS which requires particle populations to have a two or three fold difference in particle size (Filipe et al., 2010). Perhaps, NTA is more suitable for the analysis of polydisperse samples, giving a truer picture of the sample.

In some cases, NTA mean size values were larger than their DLS counterparts by a small margin. This may be explained by the lower size detection limit of DLS compared with NTA. Therefore DLS has the ability to size smaller sized particles (<30 nm) in the distribution with greater accuracy, resulting in smaller mean size values. In the case of KETO and POS, Table 2 and SI. 1 shows DLS particle sizes are greater than their NTA counterparts, a feature noted elsewhere in the literature (Filipe et al., 2010). There are a few possible explanations for this. Firstly, PDI measurements would suggest that KETO nano- dispersions are the most polydisperse of all studied API nano- dispersions i.e. multimodal and therefore may yield less reliable size data via DLS. This fact is also supported by the larger error bars associated with DLS data for KETO nano-dispersions compared with that of NTA (Fig. 2). Small error bars associated with NTA KETO samples suggest good reproducibility for these datasets (Table 2). The polydispersity of the KETO nano-dispersions (Table 2 and Fig. 2) may explain the difference in particle size values obtained for the two techniques. DLS, being an intensity based technique may not size polydisperse samples such as KETO accurately. Perhaps NTA measurements give a more realistic representation of PSDs for KETO, making NTA the more suitable technique for analysis of KETO nano-dispersions.

Both ITR and KETO DLS derived mean count rates follow a similar trend with count rates decreasing over the 30 minute period (Fig. 11a). It has been shown previously that count rates can act as a surrogate for NP concentration, however they are dependent upon both particle size and concentration (Hassan et al., 2015). Fig. 11b provides evidence of decreasing ITR particle concentration over 30 minutes according to NTA. Therefore DLS and NTA are in agreement in this respect. Fig. 11b shows KETO NTA total particle concentration is lower than ITR, however beyond 10 minutes no difference exists. It appears that DLS derived count rates can indeed be used as a surrogate for particle concentration. On the other hand other studies have concluded that NTA concentration measurements are possibly inaccurate, and perhaps this data should be considered relative rather than absolute (Gallego-Urrea et al., 2011; Krueger et al., 2016). Ultimately, the ability of NTA to provide particle concentration values remains an advantage over DLS.

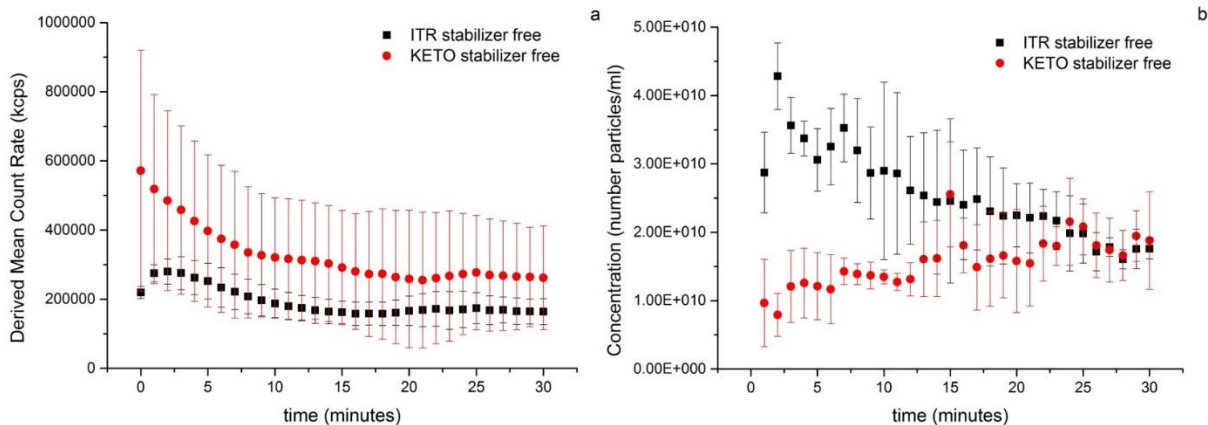


Fig. 11 (a) DLS derived mean count rate (kcps) versus time (minutes) and (b) NTA concentration (number particles/ml) versus time (minutes) for ITR and KETO stabilizer free NPs.

There may be a number of factors impacting measurements obtained via NTA and DLS. Measurements carried out using NTA involved a preparation procedure whereby NPs were formed outside of the sample chamber and quickly injected into the sample chamber upon formation. In this instance, NPs are exposed to two different environments, initial formation in sterile glass vials followed by injection via a syringe into the sample chamber. In contrast, measurements performed using DLS were truly obtained *in situ* i.e. NPs were formed inside the glass cuvette and size analysis was initiated almost instantaneously hence measurements begin at 0 minutes for the DLS datasets in contrast to 1 minute with NTA. In the case of DLS, NPs are exposed to a single homogeneous environment for the duration of the 30 minutes. NPs are also exposed to some shearing forces with NTA when undergoing injection into the sample chamber and advancing the sample, not imposed by DLS. These forces may cause breakage of particle aggregates and therefore smaller average particle size values for NTA throughout the analysis for KETO samples (Fig. 2). Sample dilution was employed for NTA analysis alone, which may also have impacted upon sedimentation rates and size distributions obtained (Philo, 2009). It is also worth noting the markedly different physical appearance of the KETO NPs as shown in photographs (Fig. SI. 5c and d). It is evident that the KETO nano-dispersions were visibly different to the other API nano-dispersions. They appeared as clear solutions both upon NP formation and by the end of the 30 minute study. POS and ITR nano-dispersions exhibited a blue “hue” typical of NPs when suspended in liquid medium (Fig. SI. 5a, b, e and f).

NTA measurements require the operator to select suitable analysis settings prior to sample measurement, a form of visual validation which is subject to operator bias (Filipe et al., 2010). The settings required for KETO NP analysis were profoundly different to that of ITR and POS (screenshot of setting can be found within Figs. SI. 26 and 27). Much higher settings were required in order to obtain a clear and suitable view of the KETO NPs for size measurements. For example, for KETO NPs stabilized with MPEG 1 mg/ml a camera level of 12 was utilised, while a camera level of 5 and 4 was used for ITR and POS equivalents. For this reason NTA sizes KETO NPs with greater difficulty.

Both techniques confirmed POS NPs were the least stable. They also confirmed DMPEG to be the best stabilizer as demonstrated by its ability to delay crystallisation for the longest period of time (Fig. 10 and Table. SI. 1). DLS studies concluded that DMPEG 1.5 mg/ml to be the most effective concentration whilst NTA favours a 1 mg/ml concentration (McComiskey et al., 2018). It may be the case that increasing DMPEG concentration up to a threshold of 1 mg/ml inhibits crystallisation therefore achieving greater NP stability. Beyond this point any further increase in concentration is of no benefit, perhaps a saturation limit is reached. The slight difference in effective concentration suggested by the two techniques can be explained by the analysis environment and the comparison of a number versus intensity based technique. There are a number of other factors to be considered when interpreting data and assessing the suitability of these sizing techniques. DLS requires little skill on the part of the operator, whilst NTA requires the operator to select suitable detection and analysis settings, which are dependent upon operator judgement and experience. In addition, NTA requires sample particle concentration to be in the range of 10^7 to 10^9 particles per ml. Therefore, determining the correct dilution factor can be time consuming for the user, with dilution possibly impacting upon original particle properties and accurate analysis. On the other hand, DLS has the ability to adjust the attenuator employed based on sample concentration automatically removing operator bias. NTA also has the disadvantage of longer measurement time over DLS, as multiple measurements are necessary in order to obtain statistically meaningful results. Although NTA has greater peak resolution, this comes with reduced sensitivity to particles smaller than 30 nm. Samples with average particle sizes below 30 nm may be more suitable for DLS. The particle sizing technique selected should consider all prior information known

about the sample, as well as the critical sample characteristics to be determined, as these will have a great impact upon end product performance.

An obvious advantage of NTA over DLS lies in its ability to visualise sample changes *in situ*. The novel application of NTA for the purposes of monitoring the dynamic, complex journey of crystallisation *in situ* has the potential to provide researchers with lucrative information regarding the physical processes taking place during sample analysis.

5. Conclusion

Critical to the success of the NP formulation process is the utilisation of more than one particle sizing technique. This study, revealed the detailed and diverse amount of information that can be provided via particle size characterisation using both NTA and DLS for nano-dispersions. Both techniques concluded ITR NPs were the most stable and POS NPs the least stable. Both techniques confirmed DMPEG was the most effective stabilizer for POS nano-dispersions. It seems that a number of large sized particles within the nano-dispersions have a profound impact upon the mean particle size measured using DLS. Hence, DLS and NTA sizing techniques should be used in a complimentary manner, making it possible to characterise nano-dispersions in a quick and detailed way. Combining information derived via both techniques provides the user with the opportunity to gain a complete holistic picture of the sample under analysis. The suitability of the particle sizing technique utilised is dependent upon the sample in question undergoing analysis as well as critical sample characteristics to be determined. For the first time, NTA was successfully utilised for the innovative purpose of *in situ* monitoring of crystal growth via “non-classical crystallisation” pathways. Mie theory was successfully employed to explain the relationship between material composition and particle light scattering power. This finding can provide an alternative means to conventional methods for assessing the progress of the dynamic crystallisation process on the nano-scale in real time. Such information can serve to deepen our understanding of these complex physical processes.

6. Acknowledgements

Research leading to these results was supported by the Synthesis and Solid State pharmaceutical Centre (SSPC), financed by a research grant from Science Foundation Ireland (SFI) and co-funded under the European Regional Development Fund (Grant Number 12/RC/2275). The authors would like to thank Dr. Grzegorz Garbacz (Physiolution GmbH, Germany) for kindly supplying itraconazole.

7. References

- Anderson, W., Kozak, D., Coleman, V.A., Jämting, Å.K., Trau, M., 2013. A comparative study of submicron particle sizing platforms: Accuracy, precision and resolution analysis of polydisperse particle size distributions. *J. Colloid Interface Sci.* 405, 322–330. doi:10.1016/j.jcis.2013.02.030
- Bell, N.C., Minelli, C., Tompkins, J., Stevens, M.M., Shard, A.G., 2012. Emerging techniques for submicrometer particle sizing applied to stober silica. *Langmuir* 28, 10860–10872. doi:10.1021/la301351k
- Berne, B., Pecora, R., 2000. *Dynamic light scattering with applications to chemistry, biology and physics.* Mineola, Dover.
- Bootz, A., Vogel, V., Schubert, D., Kreuter, J., 2004. Comparison of scanning electron microscopy, dynamic light scattering and analytical ultracentrifugation for the sizing of poly(butyl cyanoacrylate) nanoparticles. *Eur. J. Pharm. Biopharm.* 57, 369–375. doi:10.1016/S0939-6411(03)00193-0
- Brown, P.H., Schuck, P., 2006. Macromolecular size-and-shape distributions by sedimentation velocity analytical ultracentrifugation. *Biophys. J.* 90, 4651–4661. doi:10.1529/biophysj.106.081372
- Calzolari, L., Gilliland, D., Garcia, C.P., Rossi, F., 2011. Separation and characterization of gold nanoparticle mixtures by flow-field-flow fractionation. *J. Chromatogr. A* 1218, 4234–4239. doi:10.1016/j.chroma.2011.01.017
- Carlton, R.A., 2011. *Pharmaceutical Microscopy.* doi:10.1007/978-1-4419-8831-7
- Demeester, J., Smedt, S., Sanders, N., Haustraete, J., 2005. Light Scattering, in: Jiskoot, W., Crommelin, D.J. (Ed.), *Methods for Structural Analysis of Protein Pharmaceuticals.* Arlington: AAPS.
- Dragovic, R.A., Gardiner, C., Brooks, A.S., Tannetta, D.S., Ferguson, D.J.P., Hole, P., Carr, B., Redman, C.W.G., Harris, A.L., Dobson, P.J., Harrison, P., Sargent, I.L., 2011. Sizing and phenotyping of cellular vesicles using Nanoparticle Tracking Analysis. *Nanomedicine Nanotechnology, Biol. Med.* 7, 780–788. doi:10.1016/j.nano.2011.04.003
- Einstein, A., 1908. Elementare theorie der brownischen bewegung. *Zeitschrift für Elektrochemie und Angew. Phys. Chemie* 14, 235–239.
- Filipe, V., Hawe, A., Jiskoot, W., 2010. Critical evaluation of nanoparticle tracking analysis (NTA) by NanoSight for the measurement of nanoparticles and protein aggregates. *Pharm. Res.* 27, 796–810. doi:10.1007/s11095-010-0073-2
- Gallego-Urrea, J.A., Tuoriniemi, J., Hassellöv, M., 2011. Applications of particle-tracking analysis to the determination of size distributions and concentrations of nanoparticles in environmental, biological and food samples. *TrAC - Trends Anal. Chem.* 30, 473–483. doi:10.1016/j.trac.2011.01.005
- Hahn, D.W., 2009. Light Scattering Theory. *Aerosp. Eng.* 27, 1–13. doi:dwhahn@ufl.edu

- Han, T.Y.-J., Aizenberg, J., 2007. Calcium Carbonate Storage in Amorphous Form and Its Template-Induced Crystallization. *Chem. Mater.* 20, 1064–1068. doi:dx.doi.org/10.1021/cm702032v
- Hassan, P., Rana, S., Verma, G., 2015. Making sense of brownian motion: colloid characterization by dynamic light scattering. *Langmuir* 31, 3–12. doi:10.1021/la501789z
- Joubert, M.K., Luo, Q., Nashed-Samuel, Y., Wypych, J., Narhi, L.O., 2011. Classification and characterization of therapeutic antibody aggregates. *J. Biol. Chem.* 286, 25118–25133. doi:10.1074/jbc.M110.160457
- Krueger, A.B., Carnell, P., Carpenter, J.F., 2016. Characterization of Factors Affecting Nanoparticle Tracking Analysis Results With Synthetic and Protein Nanoparticles. *J. Pharm. Sci.* 105, 1434–1443. doi:10.1016/j.xphs.2016.02.005
- Lin, H.O., Baenziger, N.C., Guillory, J.K., 1974. Physical properties of four polymorphic forms of sulfanilamide I: Densities, refractive indexes, and X-ray diffraction measurements. *J. Pharm. Sci.* 63, 145–146. doi:10.1002/jps.2600630140
- Luo, P., Roca, A., Tiede, K., Privett, K., Jiang, J., Pinkstone, J., Ma, G., Veinot, J., Boxall, A., 2016. Application of nanoparticle tracking analysis for characterising the fate of engineered nanoparticles in sediment-water systems. *J. Environ. Sci. (China)* 64, 62–71. doi:10.1016/j.jes.2016.07.019
- McComiskey, K.P.M., Mugheirbi, N.A., Stapleton, J., Tajber, L., 2018. In Situ Monitoring of Nanoparticle Formation: Antisolvent Precipitation of Azole Anti-fungal Drugs. *Int. J. Pharm.* doi:https://doi.org/10.1016/j.ijpharm.2018.03.054
- McKinlay, K.J., Allison, F.J., Scotchford, C.A., Grant, D.M., Oliver, J.M., King, J.R., Wood, J.V., Brown, P.D., 2004. Comparison of environmental scanning electron microscopy with high vacuum scanning electron microscopy as applied to the assessment of cell morphology. *J. Biomed Mater Res Part A* 69, 359–366.
- Mugheirbi, N.A., Tajber, L., 2015. Mesophase and size manipulation of itraconazole liquid crystalline nanoparticles produced via quasi nanoemulsion precipitation. *Eur. J. Pharm. Biopharm.* 96, 226–236. doi:10.1016/j.ejpb.2015.08.005
- Niederberger, M., Cölfen, H., 2006. Oriented attachment and mesocrystals: non-classical crystallization mechanisms based on nanoparticle assembly. *Phys. Chem. Chem. Phys.* 8, 3271–3287. doi:10.1039/b604589h
- Palmberger, S., Mohr, C., Stubauer, G., 2015. Patent Application Publication Pub. No.: US 2017/0139001 A1.
- Peeters, O.M., Blaton, N.M., De Ranter, C.J., 1996. (cis)-2-(sec)-Butyl-4-(4-(4-((2-(2,4-dichlorophenyl)-2-(1H)-1,2,4-triazol-1-ylmethyl)-1,3-dioxolan-4-yl)methoxy)phenyl)-1-piperazinyl)phenyl)-2,4-dihydro-3H-1,2,4-triazol-3-one (Itraconazole). *Acta Crystallogr. Sect. C* 52, 2225–2229. doi:10.1107/S0108270196004180
- Peeters, O.M., Blaton, N.M., De Ranter, C.J., 1979. (cis)-1-Acetyl-4-(4-((2-(2,4-dichlorophenyl)-2-(1H)-1-imidazolylmethyl)-1,3-dioxolan-4-yl)methoxy)phenyl)piperazine: ketoconazole. A crystal structure with disorder. *Acta Crystallogr. Sect. B* 35, 2461–2464. doi:10.1107/S0567740879009651
- Peeters, O.M., Blaton, N.M., Gerber, J.G., Gal, J., 2004. (+)-(cis)-1-Acetyl-4-(4-(((2(R),4(S))-2-(2,4-dichlorophenyl)-2-(1H)-imidazol-1-ylmethoxy)-1,3-dioxolan-4-yl)methoxy)phenyl)piperazine [(2(R),4(S))-(+)-ketoconazole]. *Acta Crystallogr. Sect. E* 60, o367–o369. doi:10.1107/S1600536804003046
- Philo, J.S., 2009. A critical review of methods for size characterization of non-particulate

- protein aggregates. *Curr Pharm Biotechnol.* 10, 359–372.
- Pouget, E.M., Bomans, P.H.H., Goos, J.A.C.M., Frederik, P.M., de With, G., Sommerdijk, N.A.J.M., 2009. CaCO₃ Formation Revealed by Cryo-TEM. *Science* (80-.). 323, 1455–1458. doi:doi: 10.1126/science.1169434
- Radha, A.V., Forbes, T.Z., Killian, C.E., Gilbert, P.U.P.A., Navrotsky, A., 2010. Transformation and crystallization energetics of synthetic and biogenic amorphous calcium carbonate. *Proc. Natl. Acad. Sci. U. S. A.* 107, 16438–16443. doi:10.1073/pnas.1009959107
- Singh, S., Dunmur, D.A., 2002. Liquid Crystal: Fundamentals, in: *Liquid Crystals: Fundamentals*. p. 62.
- Svedberg, T., 1906. Über die eigenbewegung der teilchen in kolloidalen losungen. *Zeitschrift für Elektrochemie und Angew. Phys. Chemie* 12, 853–860.
- Tarnacka, M., Adrjanowicz, K., Kaminska, E., Kaminski, K., Grzybowska, K., Kolodziejczyk, K., Wlodarczyk, P., Hawelek, L., Garbacz, G., Kocot, A., Paluch, M., 2013. Molecular dynamics of itraconazole at ambient and high pressure. *Phys. Chem. Chem. Phys.* 15, 20742–20752. doi:10.1039/C3CP52643G
- Touzet, A., Pfefferlé, F., der Wel, P. van, Lamprecht, A., Pellequer, Y., 2018. Active freeze drying for production of nanocrystal-based powder: A pilot study. *Int. J. Pharm.* 536, 222–230. doi:10.1016/j.ijpharm.2017.11.050
- Watanabe, A., Ohnuma, N., 2000. Crystallographic characteristics of crystal habits and their peculiarity to the substance (study of crystalline drugs by means of a polarizing microscope). *J. Pharm. Soc. Japan* 120, 290–297.
- Wong, J., Papadopoulos, P., Werling, J., Rebbeck, C., Doty, M., Kipp, J., Konkell, J., Neuberger, D., 2006. Itraconazole suspension for intravenous injection: determination of the real component of complete refractive index for particle sizing by static light scattering. *PDA J Pharm Sci Technol* 60(5), 302–313.
- Yang, D.T., Lu, X., Fan, Y., Murphy, R.M., 2014. Evaluation of Nanoparticle Tracking for Characterization of Fibrillar Protein Aggregates. *AIChE J.* 60, 1236–1244. doi:10.1002/aic.14349
- Wittbold, W., Tatarkiewicz, K., 2017. Biological Characterization Using Protein Crystal Measurements. *BioProcess International* 15(3), 48-51.
- Zölls, S., Tantipolphan, R., Wiggenhorn, M., Winter, G., Jiskoot, W., Friess, W., Hawe, A., 2012. Particles in therapeutic protein formulations, Part 1: Overview of analytical methods. *J. Pharm. Sci.* 101, 914–935. doi:10.1002/jps.23001